Epilepsy & Behavior 38 (2014) 71–80

Contents lists available at ScienceDirect

Epilepsy & Behavior

journal homepage: www.elsevier.com/locate/yebeh

Review

Brain complex network analysis by means of resting state fMRI and graph analysis: Will it be helpful in clinical epilepsy?

Heloisa Onias [a], Aline Viol [b], Fernanda Palhano-Fontes [a], Katia C. Andrade [a], Marcio Sturzbecher [c], Gandhimohan Viswanathan [b], Draulio B. de Araujo [a,*]

[a] Brain Institute/Onofre Lopes University Hospital, Federal University of Rio Grande do Norte (UFRN), Natal, Brazil
[b] Department of Physics, UFRN, Natal, Brazil
[c] Department of Physics, University of Sao Paulo, Ribeirao Preto, Brazil

ARTICLE INFO

Article history:
Revised 11 October 2013
Accepted 16 November 2013
Available online 27 December 2013

Keywords:
Complex network
Graph
fMRI
Resting state
Epilepsy

ABSTRACT

Functional magnetic resonance imaging (fMRI) has just completed 20 years of existence. It currently serves as a research tool in a broad range of human brain studies in normal and pathological conditions, as is the case of epilepsy. To date, most fMRI studies aimed at characterizing brain activity in response to various active paradigms. More recently, a number of strategies have been used to characterize the low-frequency oscillations of the ongoing fMRI signals when individuals are at rest. These datasets have been largely analyzed in the context of functional connectivity, which inspects the covariance of fMRI signals from different areas of the brain. In addition, resting state fMRI is progressively being used to evaluate complex network features of the brain. These strategies have been applied to a number of different problems in neuroscience, which include diseases such as Alzheimer's, schizophrenia, and epilepsy. Hence, we herein aimed at introducing the subject of complex network and how to use it for the analysis of fMRI data. This appears to be a promising strategy to be used in clinical epilepsy. Therefore, we also review the recent literature that has applied these ideas to the analysis of fMRI data in patients with epilepsy.

This article is part of a Special Issue entitled "NEWroscience 2013".

1. Introduction

Complex systems consist of a large number of elements that mutually interact and that exhibit global behaviors or emergent proprieties not deducible from a simple local analysis. Such systems are not guided by central control, but rather they present self-organizing collective dynamics [1]. The notion of complex networks emerges in this context. Any complex system described mathematically by graph theory can be called a complex network [2]. In recent years, complex networks have become of major interest in the biological, technological, and social sciences, such as ecological networks, science of collaboration networks, the World Wide Web, social networks, and neuroscience [3], just to mention a few.

On the other hand, the advent of functional neuroimaging tools opened an important window for the noninvasive investigation of the human brain, among which functional magnetic resonance imaging (fMRI) plays a prominent role. It is capable of evaluating different brain sites over time, which is the basic need for the use of complex network strategies. In fact, the union of these two techniques has led to interesting results from basic [4,5] to clinical neuroscience [6–8].

Considering the growing number of studies in this area, we herein aim at providing an introduction to complex networks and a guideline of its application for the analysis of functional connectivity fMRI data. Furthermore, we review the recent literature that has applied these ideas to the analysis of fMRI data in patients with epilepsy.

2. Functional magnetic resonance imaging

Functional magnetic resonance imaging is based on the observation that the increase in neuronal electrical activity in a particular site is accompanied by a local increase in cerebral blood flow at the arteriole level [9]. This leads to a slight modulation of the MRI signal that gives rise to the contrast mechanism known as BOLD (blood oxygenation level-dependent) [10].

Typical fMRI experiments involve the serial acquisition of MRI scans with BOLD contrast images of the whole brain being collected every 1–2 s (depending on the repetition time —TR). Because of the low amplitude of such evoked signals (typically on the order of 3%), usually the subjects are asked to perform the same task several times, and a sophisticated strategy of analysis is employed to accurately detect statistically significant activated brain areas [11–17].

This technique has just completed 20 years [18]. It has been a reference tool in a broad range of human brain studies including higher

* Corresponding author at: Brain Institute (UFRN), Av. Nascimento de Castro, 2155, 59056-450 Natal, RN, Brazil.
E-mail address: draulio@neuro.ufrn.br (D.B. de Araujo).

1525-5050/$ – see front matter © 2013 Elsevier Inc. All rights reserved.
http://dx.doi.org/10.1016/j.yebeh.2013.11.019

cognitive processes [19], pharmacological challenges [20,21], and clinical applications [22], as in the case of epilepsy [23].

Currently, fMRI plays an important role in assisting surgical treatment of patients with epilepsy [23]. Traditionally, it involves noninvasive functional preoperative mapping of eloquent areas such as the ones related to motor, language, and memory systems [23–25], as well as determining lateralization of receptive (Wernicke's area) and expressive (Broca's area) language fields [26]. However, these approaches are not of much help when it comes to the precise spatial localization of the epileptic activity, which is a central issue in the diagnosis and treatment of epilepsy. More recently, however, resting state fMRI has appeared as a promising approach.

Resting state fMRI focuses on spontaneous fluctuations of the BOLD signal, or the "intrinsic activity" of the brain, instead of looking at evoked activity. The term "intrinsic activity" summarizes any ongoing neural and metabolic activity that is not directly correlated to a specific task. It is usually recorded with the subject lying down relaxed with their eyes closed, without falling asleep, while continuous fMRI data are being collected [27].

Nowadays, several studies are using this approach to examine the existence and extent of intrinsic functional connections between brain regions, known as functional connectivity fMRI (fc-fMRI). These methods can be divided into two main groups: model-dependent or model-free. In the model-dependent method, regions of interest (seeds) are chosen based on a priori knowledge/question, from which time series are extracted and processed, aiming at evaluating if this region is functionally connected to other brain areas [28,29]. In the time domain, two mathematical approaches are frequently used: cross-correlation analysis (Pearson or partial correlation) and statistical parametric mapping [30–32]. One of the main disadvantages of these two approaches is that both are sensitive to the shape of the hemodynamic response, which is known to vary among different individuals and brain regions and with age [33–35]. Moreover, contamination from physiological processes, such as respiratory and cardiac oscillations, can lead to false high correlations [36,37]. To overcome these problems, one can use coherence, which is the representation of correlation in the frequency domain, to create functional maps that define functional connectivity of predefined brain regions. Although these maps provide information about the functional connectivity of the seeds, they cannot be used to study functional connectivity at a whole-brain scale. For this purpose, model-free methods can be used, as independent component analysis (ICA), principal component analysis (PCA), and clustering [28,38,39].

Besides functional connectivity, effective connectivity, the causal influence that a neural unit exerts over another, has also been the focus of attention. Two main techniques have been used: Granger causal modeling (GCM) and dynamic causal modeling (DCM). In the GCM, it is assumed that if one time series is a time-shifted version of the other, then the one with temporal precedence caused the other, giving a measure of directionality [27,40]. On the other hand, DCM is a hypothesis-led approach to study observed brain responses, in which hypotheses are outlined in a reasonably realistic neuronal model of interacting cortical regions (networks), and a Bayesian model is used to quantify the influence of one network over the other [41].

In addition to evaluating differences of functional or effective connectivity between pairs of brain regions, resting state fMRI is being progressively used to better understand how brain networks interact, using the framework of complex networks.

3. Brain complex networks

Although the study of complex networks is mathematically based on graph theory [42], the study of large-scale complex systems led to the development (and definitions) of new metrics and statistical observables. It is worth noting that the nomenclature may change according to the field of application, and, frequently, the terms "graph" and "network" are used synonymously. We have chosen to adopt, in what follows, the term "network" for all concepts related to networks and graphs. In this section, we introduce the basic terminology and quantities important in the science of complex networks.

A network is a way to code a set of elements together with their relations. The elements are defined as nodes (or vertices), and their

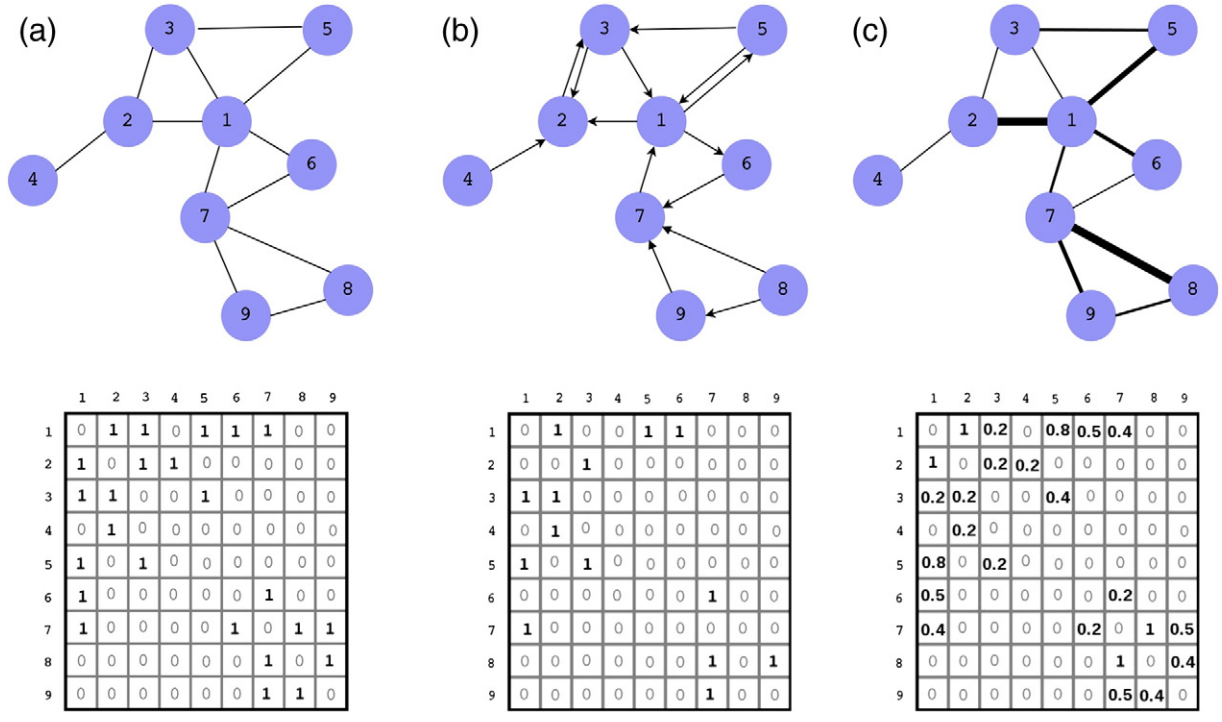

Fig. 1. Types of networks. Examples of undirected (a), directed (b), and weighted (c) networks and their corresponding adjacency matrices. See Refs. [2,49] for a more detailed introduction on complex networks.

relations are defined as links (or edges) [2]. For example, if nodes represent people in a social network, then links can represent friendships between pairs of people. Mathematically, a network is represented by ordered pairs of set $G(N,l)$ in which N is a set of nodes and l is a set of links. Graphically, the nodes are plotted as points and the links as lines joining them [2] (Fig. 1).

When two nodes are connected by a link, they are considered neighbors (or adjacent). A network with N nodes is said to have order N. A network structure that assigns a label (weight) to each link is called a weighted network. Otherwise, if the links of a network do not have labels, the network is called binary (or unweighted).

A common and very useful representation of a network is the adjacency matrix (or connection matrix), which completely defines the topology of the network. The matrix element $a(i,j)$ is nonzero if there is a link between nodes i and j. In binary adjacent matrices, the link between nodes i and j is represented by 1 and no connection by 0 (Fig. 1a). When the adjacency matrix is weighted and normalized, the value of $a(i,j)$ will lie in the interval from 0 to 1 (Fig. 1c). Moreover, network links can be classified as undirected or directed (Fig. 1b). In an undirected network, the number of links in a node, k, is the degree of this node. In directed network, the in-degree and the out-degree correspond to the number of in-coming and out-coming links, respectively. In this case, the sum of in-degree and out-degree is the degree of a node, k (Fig. 1b). The average degree of all nodes is the degree of network. Since most of the studies in brain networks have been carried out with binary undirected networks, we will focus on this class of networks.

3.1. Degree distribution

The degree distribution $P(k)$ is the normalized frequency histogram of the node degrees for the network (see Eq. (2) in Table 1), such that $P(k)$ is the probability that a randomly chosen node has degree equal to k [42] (Fig. 2). This definition is important because it contains information about network architecture and can be crucial for identifying the type of network [42]. For example, a heavy-tailed distribution

Table 1
Complex network measures: Equations and definitions.

Measure	Equation		Definitions
Degree of node [7]	$k_i = \sum_{j \in G} a(i,j)$	(1)	G represents the full set of network. $a(i,j)$ is the element of adjacency matrix. $a(i,j) = 1$ when there is a link between nodes i and j. $a(i,j) = 0$ otherwise.
Degree distribution [2]	$P(k) = \frac{n_k}{N}$	(2)	n_k is the total number of nodes with degree k. N is the total number of nodes.
Cost or probability of connection [7]	$P_{cost}(G) = \frac{1}{N(N-1)} \sum_{i \in G} k_i$	(3)	This metric is evaluated in the full network. G represents the network.
Cluster coefficient [47]	$C(G) = \frac{1}{N} \sum_{i \in V} C(i) = \frac{1}{N} \sum_{(i,j,h) \in G} \frac{2a(i,j)a(i,h)a(j,h)}{k_i(k_i-1)}$	(4)	$C(i)$ is the cluster coefficient of node i. $C(i) = 0$ for $k_i < 3$.
Transitivity [47]	$T(G) = \frac{\sum_{i \in G} 2a(i,j)a(i,h)a(j,h)}{\sum_{i \in G} k_i(k_i-1)}$	(5)	Unlike cluster coefficient, this metric is defined only to a full network.
Local efficiency [7]	$E_{local}(i) = \frac{1}{N_{G_i}\left(N_{G_i}-1\right)} \sum_{j,k \in G_i} \frac{1}{d(j,k)}$	(6)	G_i is a set of neighbors of i.
Shortest path length [47]	$L = \frac{1}{N(N-1)} \sum_{i,j \in G, i \neq j} d(i,j)$	(7)	Where $d(i,j)$ is the shortest path length between i and j.
Global efficiency [7]	$E_{global}(G) = \frac{1}{N(N-1)} \sum_{i \neq j \in G} \frac{1}{d(i,j)}$	(8)	E_{global} is evaluated in the full network.
"Small-worldness" [53]	$\sigma = \frac{C/C_{rand}}{L/L_{rand}}$	(9)	C_{rand} and L_{rand} are cluster coefficient and shortest path length evaluated to randomly network from original network. The network is small-world if $\sigma \gg 1$

The equations in this table refer to binary undirected networks.

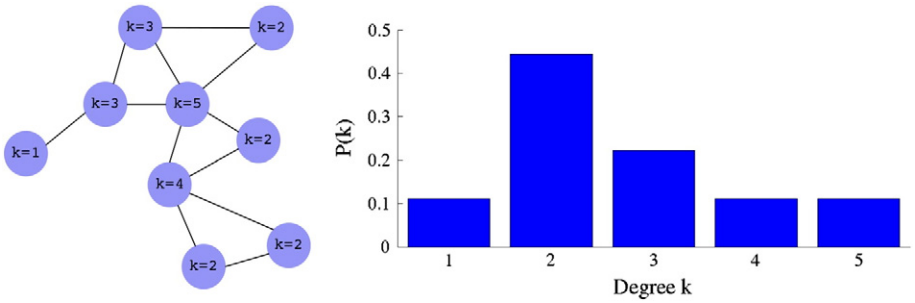

Fig. 2. Degree distribution. Illustrative example showing the degree of each node and, on the right, the degree distribution of the network.

indicates the existence of highly connected nodes, known as hubs, and their presence influences its information exchange efficiency and the network resilience, i.e., if a node is removed, the structure of the network will not change much qualitatively [43].

3.2. The cluster coefficient

The distribution of information processing in brain networks can be understood through the concept of functional segregation, and a possible way to infer this property is by quantifying how clustered the network is.

The concept of cluster is quite simple. If the nearest neighbors of a node are also directly connected to each other, they form a cluster. In the example of social networks, the friend of your friend is likely also your friend [44]. The clustering coefficient of a node, $C(i)$, is the ratio of the number of links that exist between the nearest neighbors of the chosen node and the number of possible links between them [45] (Fig. 3a).

The clustering coefficient of a network, $C(G)$, is the average over the clustering coefficient of all nodes (see Eq. (4) in Table 1). Clustering coefficient values lies in the range from 0 to 1. Densely interconnected neighbors yield high clustering coefficients, while sparsely interconnected neighbors return low coefficients. Networks with high clustering coefficient have larger resilience.

Another way to measure the clustering is by transitivity $T(G)$ (sometimes also called clustering coefficient) (see Eq. (5) in Table 1). The original definition of transitivity comes from social science and indicates how much a network is clustered [44]. This formulation denotes the fraction of triples of nodes present in a network that form a cluster. Transitivity and the clustering coefficient capture the same intuition of clustering, but they are of different quantities [44].

3.3. Characteristic path length

Another fundamental property of brain networks is functional integration, which indicates how integrated a network is and, thus, how easily information flows [46]. A common approach to estimate the potential for functional integration between nodes is based on the concept of path length [46] (Fig. 3b).

The shortest path length $d(i,j)$ (also called distance or geodesic path) is defined as the minimum number of links that must be traversed to go from node i to node j [45] (see Eq. (7) in Table 1). By definition, $d(i,j) \geq 1$. Therefore, $d(i,j) = 1$ if i and j are neighbors, whereas $d(i,j) \to \infty$ if the nodes are disconnected. The average of the shortest path length between all pairs of nodes in a network is called the characteristic path length (L). Small characteristic path length implies stronger potential for integration [46].

3.4. Cost

It is reasonable to admit that the greater the number of links, the higher its integration and, consequently, its efficiency. In contrast, in any real network, there is a price to pay for each additional link. This price is measured by the density of links, which is known as cost or connection probability (see Eq. (3) in Table 1). If the cost is low, the network is considered economic [44].

3.5. Efficiency

Assuming a parallel flux of information, the efficiency of communication between two nodes is defined to be inversely proportional to the shortest path length, $\varepsilon(i,j) = 1/d(i,j)$ [47]. Consistently, $d(i,j) \to \infty$, return $\varepsilon(i,j) = 0$, and the efficiency is maximum, $\varepsilon(i,j) = 1$, when $d(i,j) = 1$. The efficiency of a set of nodes is the sum of the efficiencies of all node pairs, normalized by maximal number of links $N(N-1)/2$.

When the set of nodes includes all nodes, then the resulting efficiency is known as the global efficiency, E_{global} (see Eq. (8) in Table 1) [7]. Local properties can also be characterized by taking subgroups only with neighbors of each node in choosing the set of nodes. The average of all such subgroups of the network is the local efficiency, E_{local}, of the network (see Eq. (6) in Table 1). The local efficiency reveals how

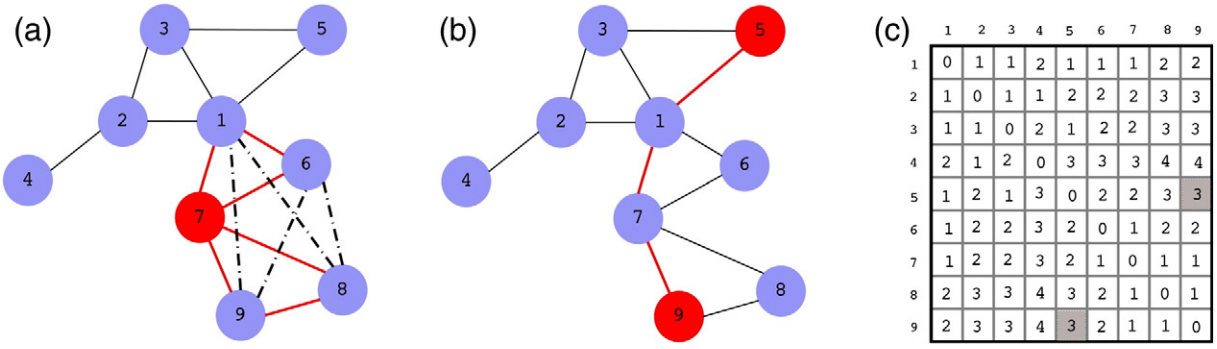

Fig. 3. Cluster coefficient and path Length. (a) A representation of the cluster coefficient of node 7 (red) and all possible connections between its neighbors by a dashed line is displayed. (b) A graphical representation of shortest path length between nodes 5 and 9 (thick line) and (c) its path length matrix (or distance matrix).

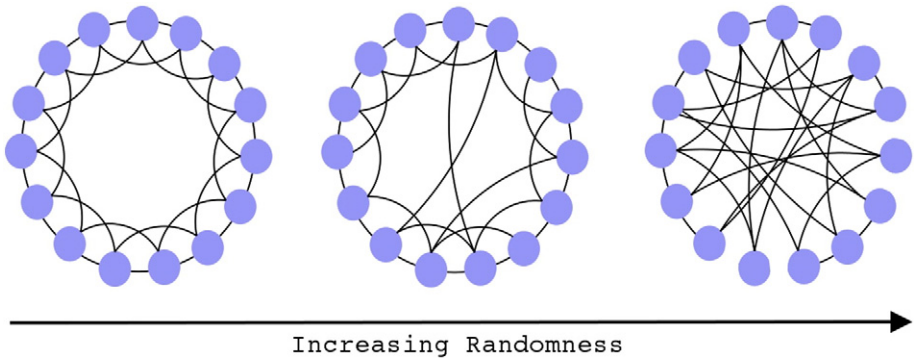

Fig. 4. The Watts–Strogatz model of the small-world. The network on the left represents a ring lattice with circular boundary conditions. The initial configuration connections are randomly rewired with a given rewiring probability p. For $p = 0$ (no rewiring), the network retains its regular lattice topology. For $p = 1$, the network is completely random (network at right), and all lattice features disappear. Intermediate values of p result in networks that consist of a mixture of random and regular network (at the center where the small-world phenomenon emerges) [45].

efficient the communication is between the first neighbors of a node when it is removed [47].

Global efficiency is a measurement of functional integration, while local efficiency is associated with functional segregation. They are alternative metrics to clustering coefficient and characteristic path length [48].

3.6. Random networks

Random networks are commonly defined as networks in which the links are randomly distributed [1]. The most famous model of random networks was proposed by Erdös and Rényi and consists of networks such that the links are distributed randomly with constant probabilities of connection between two nodes (see Ref. [2] for details). Thus, by varying the numbers of nodes and probabilities of connection, different types of networks can be constructed [42]. However, it is only one among many possible random models. In a more general definition, the random network is a model in which some chosen parameters assume fixed values, while other parameters of network are free to vary randomly [49].

3.7. Small-world

A ubiquitous network architecture that deserves attention is the small-world network. The concept of small-world emerged in the late 1960s, in a social system study by Stanley Milgram, which led to the popular expression "six degrees of separation" [50]. It characterizes how efficiently the information is exchanged over a network [47].

The idea was prominently inserted in the context of complex networks by a study of Watts and Strogatz, in which it was shown that real networks are neither completely regular nor completely random, but stays between these two extremes [45] (Fig. 4). Regular networks can be seen as the opposite of random graphs. They present an ordered structure with high clustering and high characteristic path length, while random graphs are characterized by a low clustering coefficient and low path length (Fig. 4). Therefore, in order for a network to be classified as small-world, it needs a characteristic path length similar to a random network $L \sim L_{rand}$ but a substantially higher clustering coefficient, $C \gg C_{rand}$ [6].

In an attempt to refine this measurement, Humphries and Gurney proposed the "small-worldness" metric, σ (see Eq. (9) in Table 1). In this formulation, the network is classified as small-world if $\sigma > > 1$ [51]. It is important to emphasize, however, that in order to compare small-world behavior of several networks, it is indispensable to analyze clustering coefficient and characteristic path length apart, since σ cannot capture opposite behaviors such as a concurrent increase of $L(G)$ with a decrease of $C(G)$. This architecture is of particular interest for neuroscience as brain networks of different scales exhibit small-world behavior [52].

The general idea behind the use of complex network to fMRI data is to compute the abovementioned metrics in resting state fMRI experiments. However, the implementation of such strategies is not trivial. Therefore, the next sections guide the reader throughout an example on how this is commonly conducted.

4. Complex networks and fc-fMRI

A conventional resting state fMRI protocol, as described above, is the most frequently used approach to investigate complex networks in the scenario of functional neuroimaging.

Once acquired, images have to be preprocessed using standard fMRI steps, which include slice-timing correction, head motion correction, and spatial smoothing. Moreover, most of the time, they are normalized to an anatomical standard space, such as the Montreal Neurologic Institut (MNI 152) [53].

The nodes are typically defined according to three approaches: image voxels [54], segregation based on brain functional division, and, most commonly, anatomical brain divisions [46]. In the anatomical approach, brain atlases (Fig. 5a) can be used to segment the brain into a number of subregions, which will constitute the nodes. A possible and frequently used atlas is the *Harvard-Oxford cortical and subcortical structural atlas* (with a threshold usually set at 25%). It is part of the FSL package (FMRIB Software Library, www.fmrib.ox.ac.uk/fsl), and it parcellates the brain into 110 anatomical regions (nodes) (Fig 6b).

On the other hand, the links are usually assembled as measures of functional or effective connectivity [5] between pairs of nodes. These quantities come from the time courses computed from the average HRF at each node (Fig. 6c). It is important to note that these time series are usually contaminated by a number of confounders, which come mainly from head motion, the signal from the white matter, the cerebrospinal fluid (CSF), and the global average signal[1] [55] that are thought to account for physiological noise (cardiac and respiratory). Hence, time series representing these quantities have to be regressed out from the data [56]. The remaining signal should be filtered either by a band-pass filter or by a wavelet transform. Often, the wavelet approach is chosen as biological data usually demonstrate scale invariant or fractal properties [57]. For this purpose, one can use the maximum overlap discrete wavelet transform (MODWT —www.atmos.

[1] The use of the whole-brain average signal, also called global signal, is a controversial step, and its validity is under discussion as it may introduce artifactual negative correlations.

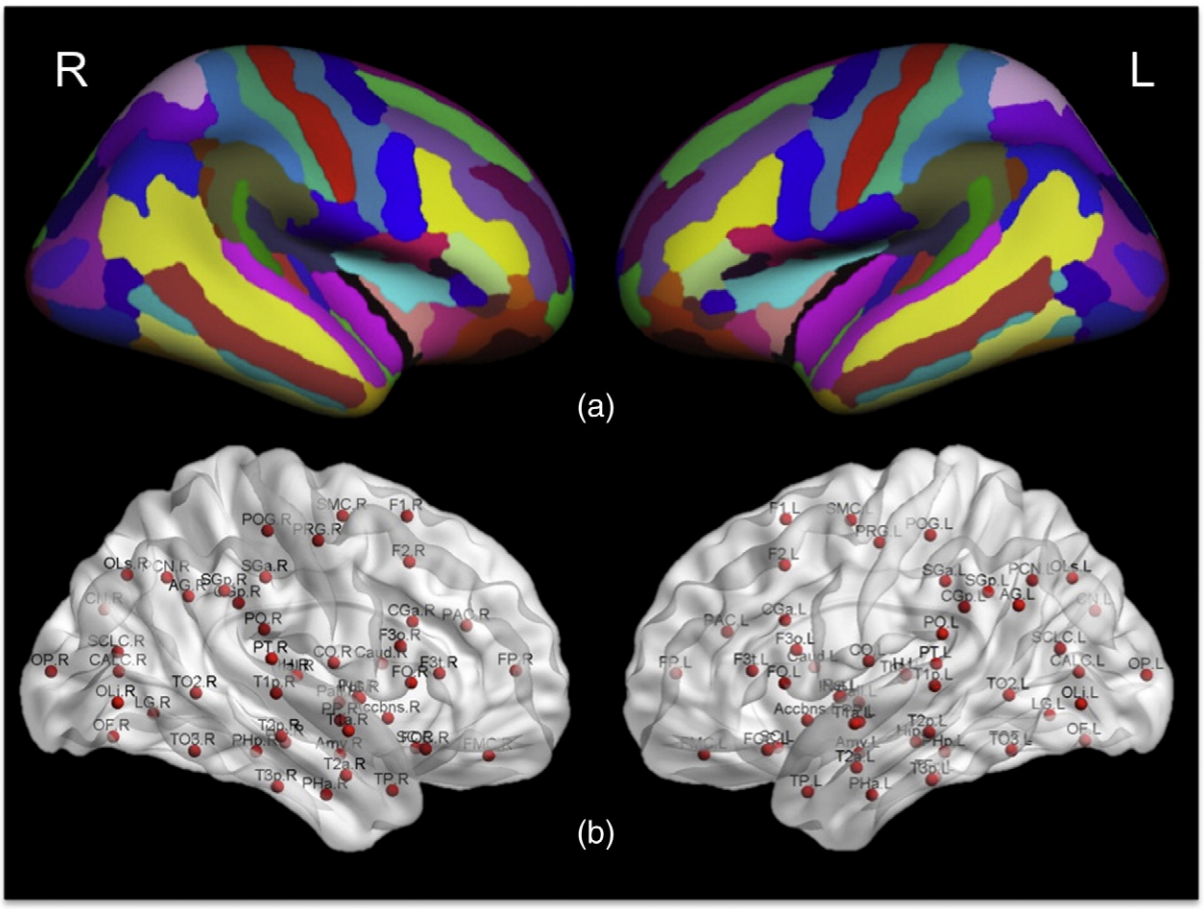

Fig. 5. Example of nodes based on anatomical regions. (a) The Destrieux atlas [76] was overlaid onto an inflated brain surface using the software FreeSurfer version 5.3.0 (https://surfer.nmr.mgh.harvard.edu/). (b) This atlas was used to define the nodes of the brain network.

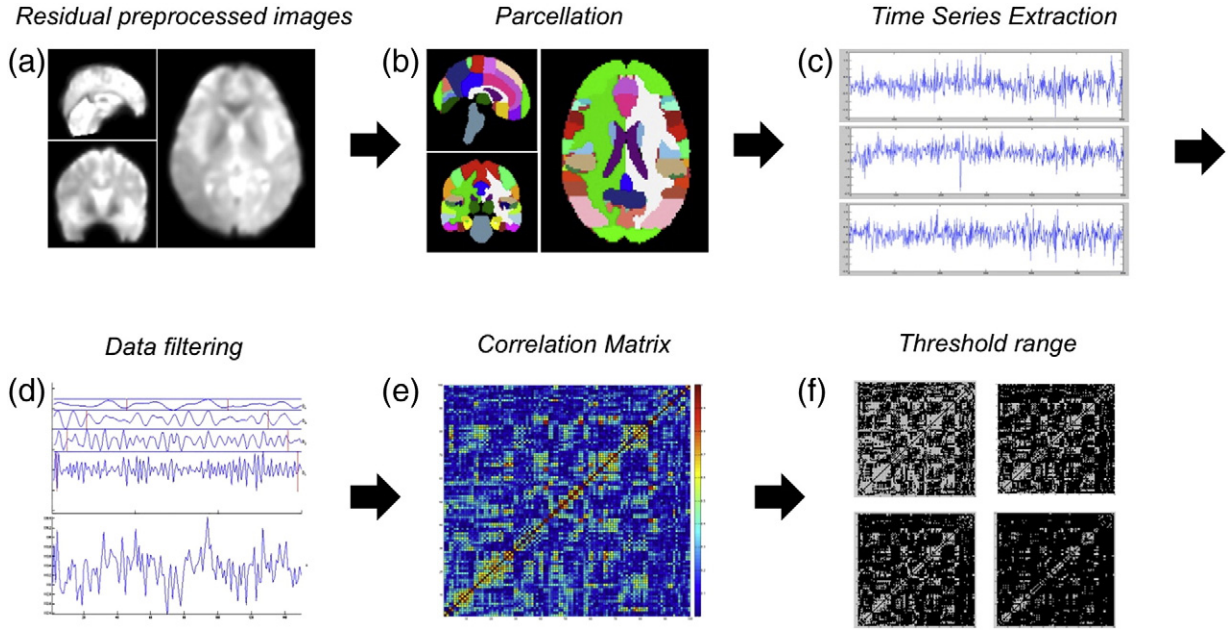

Fig. 6. A step by step illustration on how graphs from fMRI data can be generated. (a) *Residual preprocessed images* —preprocessed methods as slice-timing correction, head motion correction, spatial smoothing, and normalization are first carried out on raw fMRI data. (b) *Parcellation* —a brain atlas can be used to divide the brain in subregions. (c) *Time series extraction* —mean time series are extracted from each region to be further used to calculate the links of the network. (d) *Data filtering* —to select the frequency band of interest, the remaining signal can be filtered either by a band-pass filter or by a wavelet transform. (e) *Correlation matrix* —the correlation matrix can be constructed based on calculation of Pearson correlation coefficients between pairs of regions. (f) *Threshold range* —for each connection probability value, a binary matrix can be constructed. Smaller threshold values increase the connection probability, and more links are added to the network (more white dots), while, bigger threshold values result in less connections and, consequently, decreased connection probability (more black dots).

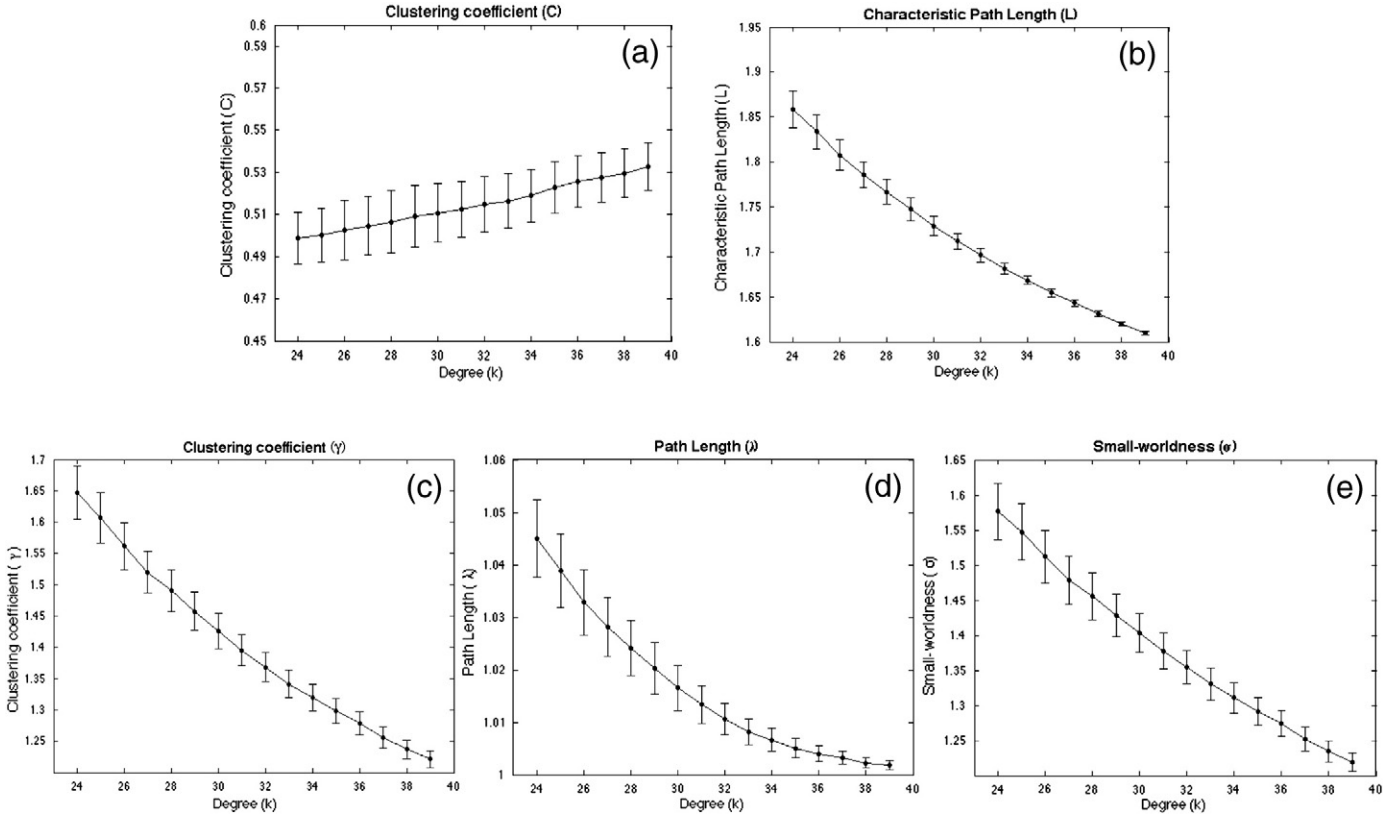

Fig. 7. Examples of topological measures. (a) Clustering coefficient (C), (b) characteristic path length (L), (c) normalized clustering coefficient ($\gamma = C/C_{rand}$), (d) normalized path length ($\lambda = L/L_{rand}$), and (e) small-worldness ($\sigma = \gamma/\lambda$). Metrics were calculated for a healthy group (7 subjects) as a function of the degree *k*. Error bars indicate standard error of the mean.

washington.edu/~wmtsa/) to divide the time series into different frequency bands (Fig. 6d). Typically, the signals are filtered in the range of approximately 0.01 to 0.1 Hz [58]. After these preprocessing steps, the remaining signal will be used to construct the links, based, for instance, on functional connectivity (Pearson correlation, see Eq. (10) in Table 1) measured between pairs of signals (nodes).

The result is an $N \times N$ (N = total number of nodes) symmetric correlation matrix (Fig. 6e), which represents the correlation coefficient (r_{xy}) between the time series of pairs of nodes, *i* and *j*. This weighted matrix can be directly used to construct a network. However, commonly this matrix is thresholded in order to obtain a binary matrix.[2] The threshold choice is of fundamental importance as it defines the topology of the network. To date, there are two common approaches for this choice [59]: (*i*) to choose a single and optimal threshold to apply to all subjects and (*ii*) to choose a range of values and describe the network proprieties as a function of the mean degree of the network.

Considering this last approach, usually the threshold range is chosen as to guarantee a small-world network regime [7]. This choice may be based on the correlation coefficient (r_{xy}) or on the connection probability (cost). In either case, the lowest threshold should be chosen to assure that the network does not have disconnected nodes. On the other end, the upper threshold should not include networks that behave like a random network. To meet this second requirement, the network needs a lower global efficiency and a larger local efficiency than its respective random network [7,60]. Therefore, individually constructed random networks are compared with the subject's adjacent matrix at a specific threshold, defining the range of interest. The result is a series of binary matrices, one for each threshold (Fig. 6f).

With all matrices in the selected range for all subjects, it is possible to calculate the desired network metrics by a number of software packages, such as the brain connectivity toolbox (www.brain-connectivity-toolbox.net [47]). Every subject will have a specific value for the metric of interest. Thus, group averages may be computed at each threshold (Fig. 7), and, further, a statistical comparison between different groups can be computed. Besides cluster coefficient (C) and path length (L), comparisons are also based on normalized values of clustering coefficient ($\gamma = C/C_{rand}$) and path length ($\lambda = L/L_{rand}$), which allows the computation of "small-worldness" (σ).

Finally, individual network topologies can be visualized for a specific threshold, which generally represent an overview of the calculated metrics. There are a number of programs designed for this purpose, such as the BrainNet Viewer (www.nitrc.org/projects/bnv) (Fig. 8).

Approaches like the ones just described have been used by several studies and have found complex network changes related to different conditions in basic neuroscience [4], neurology [8], and psychiatry [7]. For instance, graph theoretical analysis has been applied to patients with partial seizures and generalized absence seizures in order to measure topologically and organizationally changes of brain networks. To date, most of these analyses were conducted using intracranial and scalp EEG data [61–70]. Recently, a few studies have started to use these strategies on functional neuroimaging data, such as fMRI [6,71,72].

5. Complex network, fMRI, and epilepsy

Zhang et al. used diffusion tensor imaging and resting state fMRI to analyze and compare anatomical and functional whole-brain network of healthy subjects and patients with generalized tonic–clonic seizures (GTCS) [6]. In general, their findings suggest a less-optimized network organization in the patient group during interictal activity.

[2] If $r_{xy} > Th$, $r_{xy} = 1$; otherwise $r_{xy} = 0$. r_{xy} with $p < 0.05$ are also turned to zero.

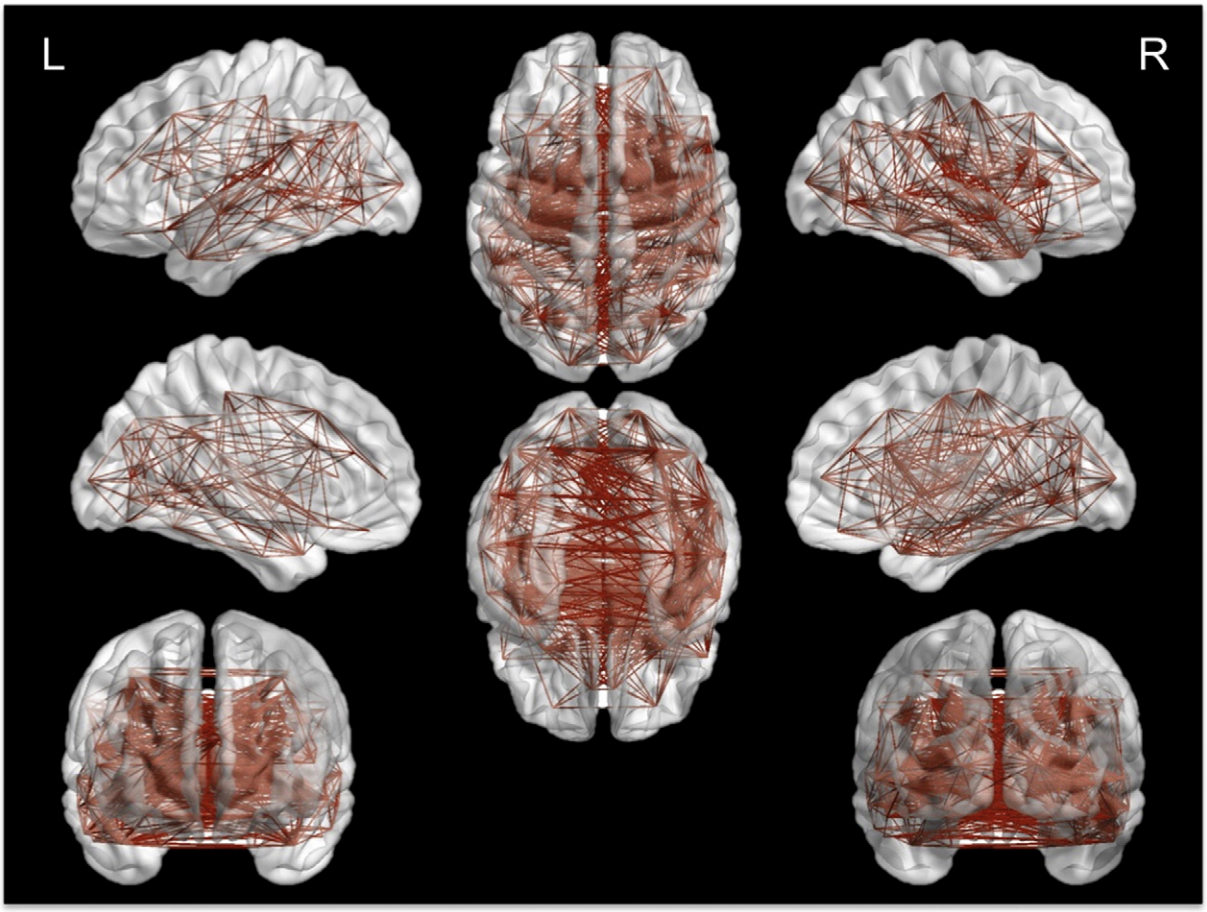

Fig. 8. Illustrative brain network of a patient with focal seizures in the left hemisphere.

This is represented by a decrease in "small-worldness" due to a decrease in the normalized clustering coefficient, with no change in normalized characteristic path length. On the other hand, patients with GTCS showed increased total connection strength in functional but not in structural connectivity. Furthermore, at the nodal level, they found a decrease in functional nodal topological properties in the brain default mode network (DMN). The amygdala showed an increase not only in functional nodal degree but also in efficiency and centrality. More interestingly, these changes were positively correlated with the duration of epilepsy. It is also worth noting that coupling of functional and structural connectivity networks was significantly decreased in IGE–GTCS, and it was negatively correlated with duration of epilepsy.

Liao et al. [71] also used resting state fMRI data to investigate functional connectivity in mesial temporal lobe epilepsy during interictal periods and, in line with Zhang and colleagues [6], observed that DMN regions have a significant decreased number of connections to other regions. Patients showed no change in normalized clustering coefficient and a decrease in normalized characteristic path length. This study also found a negative correlation of the functional connectivity between the right inferior frontal gyrus (opercular) and the left inferior frontal gyrus (triangular) with the epilepsy duration, suggesting a relationship between the decreased connectivity and the functional impairment associated with epilepsy duration.

Vlooswijk et al. [72] used fMRI with a word generation paradigm and an intelligence test to investigate brain network properties and their association with intellectual decline in patients with frontal and temporal lobe epilepsy. They observed lower values of the normalized cluster coefficient and global and local efficiency in patients when compared with healthy controls. The authors showed a diffuse disruption of small-worldness in the patient group. Interestingly, they observed that topology changes in patients with epilepsy were associated with a decline in intellectual abilities, although it is difficult to distinguish the effect of antiepileptic drugs from epilepsy itself.

6. Final remarks

Although complex networks have been successfully used in the fMRI context, there are several limitations that should be taken into account [27]. At each stage of the network construction, choices are made that determine the final metric values.

For instance, the number of regions, their sizes, and specific locations have to be chosen when nodes are constructed based on anatomy, and this will bias statistical tests [59,73]. Link representation should also be observed. They are often defined by functional connectivity measurements using a Pearson correlation coefficient. This approach, although easily implemented and commonly used in several studies, does not take into account the contribution of all other regions when calculating the pairwise correlation. An alternative approach has been the use of a partial correlation [27,74]. Another critical point is the choice of threshold. It is clear that it determines the regime of network. However, it also influences the statistical analysis [75].

Finally, and most importantly, metrics can be extracted from different conditions and diseases, using various tactics, leading to observed differences between groups. However, what are their interpretation and meaning? In fact, we believe that this question lies at the core of

the future perspective of complex network use for fMRI data and to brain sciences as a whole.

References

[1] Boccara N. Modeling complex systems. 2nd ed. New York: Springer; 2010.
[2] Caldarelli G. Scale-free networks. Complex webs in nature and technology. Oxford: OUP; 2007.
[3] Albert R, Barabasi A. Statistical mechanics of complex networks. Rev Mod Phys 2002;74:47–97.
[4] Schroter MS, Spoormaker VI, Schorer A, Wohlschlager A, Czisch M, Kochs EF, et al. Spatiotemporal reconfiguration of large-scale brain functional networks during propofol-induced loss of consciousness. J Neurosci 2012;32:12832–40.
[5] Bullmore ET, Bassett DS. Brain graphs: graphical models of the human brain connectome. Annu Rev Clin Psychol 2011;7:113–40.
[6] Zhang ZQ, Liao W, Chen HF, Mantini D, Ding JR, Xu Q, et al. Altered functional–structural coupling of large-scale brain networks in idiopathic generalized epilepsy. Brain 2011;134:2912–28.
[7] Liu Y, Liang M, Zhou Y, He Y, Hao YH, Song M, et al. Disrupted small-world networks in schizophrenia. Brain 2008;131:945–61.
[8] Stam C, Jones B, Nolte G, Breakspear M, Scheltens P. Small-world networks and functional connectivity in Alzheimer's disease. Cereb Cortex 2007;17:92–9.
[9] Roy C, Sherrington C. On the regulation of the blood-supply of the brain. J Physiol 1890;11:23.
[10] Kim SG, Ogawa S. Biophysical and physiological origins of blood oxygenation level-dependent fMRI signals. J Cereb Blood Flow Metab 2012;32:1188–206.
[11] Cabella BCT, Sturzbecher MJ, Tedeschi W, Baffa O, de Araujo DB, Neves UPD. A numerical study of the Kullback–Leibler distance in functional magnetic resonance imaging. Braz J Phys 2008;38:20–5.
[12] Cabella BCT, Sturzbecher MJ, de Araujo DB, Neves UPC. Generalized relative entropy in functional magnetic resonance imaging. Physica a-Statistical Mechanics and Its Applications 2009;388:41–50.
[13] de Araujo DB, Tedeschi W, Santos AC, Elias Jr J, Neves UP, Baffa O. Shannon entropy applied to the analysis of event-related fMRI time series. Neuroimage 2003;20:311–7.
[14] Estombelo-Montesco C, Sturzbecher M, Barros A, de Araujo D, Hussain A, I A, et al. Detection of auditory cortex activity by fMRI using a dependent component analysis. Brain Inspired Cognitive Systems 2008;l2010(657):135–45.
[15] Sturzbecher MJ, Tedeschi W, Cabella BC, Baffa O, Neves UP, de Araujo DB. Non-extensive entropy and the extraction of BOLD spatial information in event-related functional MRI. Phys Med Biol 2009;54:161–74.
[16] Tedeschi W, Muller HP, de Araujo DB, Santos AC, Neves UPC, Erne SN, et al. Generalized mutual information fMRI analysis: a study of the Tsallis q parameter. Physica a-Statistical Mechanics and Its Applications 2004;344:705–11.
[17] Tedeschi W, Muller HP, de Araujo DB, Santos AC, Neves UPC, Erne SN, et al. Generalized mutual information tests applied to fMRI analysis. Physica a-Statistical Mechanics and Its Applications 2005;352:629–44.
[18] Smith K. Brain imaging: fMRI 2.0. Nature 2012;484:24–6.
[19] Della-Justina HM, Pastorello BF, Santos-Pontelli TEG, Pontes OM, Santos AC, Baffa O, et al. Human variability of fMRI brain activation in response to oculomotor stimuli. Brain Topogr 2008;20:113–21.
[20] Del-Ben CM, Ferreira CA, Sanchez TA, Alves-Neto WC, Guapo VG, de Araujo DB, et al. Effects of diazepam on BOLD activation during the processing of aversive faces. J Psychopharmacol 2010;26:443–51.
[21] de Araujo DB, Ribeiro S, Cecchi GA, Carvalho FM, Sanchez TA, Pinto JP, et al. Seeing with the eyes shut: Neural basis of enhanced imagery following ayahuasca ingestion. Hum Brain Mapp 2012;33:2550–60.
[22] Mazzetto-Betti KC, Leoni RF, Pontes-Neto OM, Santos AC, Leite JP, Silva AC, et al. The stability of the blood oxygenation level-dependent functional MRI response to motor tasks is altered in patients with chronic ischemic stroke. Stroke 2010;41:1921–6.
[23] Duncan J. Imaging in the surgical treatment of epilepsy. Nat Rev Neurol 2010;6:537–50.
[24] Araujo D, de Araujo DB, Pontes-Neto OM, Escorsi-Rosset S, Simao GN, Wichert-Ana L, et al. Language and motor FMRI activation in polymicrogyric cortex. Epilepsia 2006;47:589–92.
[25] Banks SJ, Sziklas V, Sodums DJ, Jones-Gotman M. fMRI of verbal and nonverbal memory processes in healthy and epileptogenic medial temporal lobes. Epilepsy Behav 2012;25:42–9.
[26] Escorsi-Rosset S, Wichert-Ana L, Bianchin MM, Velasco TR, Sakamoto AC, Leitel JP, et al. Variable fMRI activation during two different language tasks in a patient with cognitive delay. Arq Neuropsiquiatr 2007;65:985–7.
[27] Smith SM. The future of FMRI connectivity. Neuroimage 2012;62:1257–66.
[28] van den Heuvel MP, Hulshoff Pol HE. Exploring the brain network: a review on resting-state fMRI functional connectivity. Eur Neuropsychopharmacol 2010;20:519–34.
[29] Li KM, Guo L, Nie JX, Li G, Liu TM. Review of methods for functional brain connectivity detection using fMRI. Comput Med Imaging Graph 2009;33:131–9.
[30] Friston K. Statistics I: experimental design and statistical parametric mapping. In: Toga A, Mazziotta J, editors. Brain mapping: the methods. Academic Press; 2002. p. 605–31.
[31] Andrade KC, Spoormaker VI, Dresler M, Wehrle R, Holsboer F, Saemann PG, et al. Sleep spindles and hippocampal functional connectivity in human NREM sleep. J Neurosci 2011;31:10331–9.
[32] van der Gaag C, Minderaa RB, Keysers C. The BOLD signal in the amygdala does not differentiate between dynamic facial expressions. Soc Cogn Affect Neurosci 2007;2:93–103.
[33] Andrade KC, Pontes-Neto OM, Leite JP, Santos AC, Baffa O, de Araujo DB. Quantitative aspects of brain perfusion dynamic induced by bold fMRI. Arq Neuropsiquiatr 2006;64:895–8.
[34] Leoni RF, Mazzeto-Betti KC, Andrade KC, de Araujo DB. Quantitative evaluation of hemodynamic response after hypercapnia among different brain territories by fMRI. Neuroimage 2008;41:1192–8.
[35] Handwerker DA, Ollinger JM, D'Esposito M. Variation of BOLD hemodynamic responses across subjects and brain regions and their effects on statistical analyses. Neuroimage 2004;21:1639–51.
[36] Shmueli K, van Gelderen P, de Zwart JA, Horovitz SG, Fukunaga M, Jansma JM, et al. Low-frequency fluctuations in the cardiac rate as a source of variance in the resting-state fMRI BOLD signal. Neuroimage 2007;38(2):306–20.
[37] Birn RM. The role of physiological noise in resting-state functional connectivity. Neuroimage 2012;62:864–70.
[38] McKeown MJ, Makeig S, Brown GG, Jung TP, Kindermann SS, Bell AJ, et al. Analysis of fMRI data by blind separation into independent spatial components. Hum Brain Mapp 1998;6:160–88.
[39] van de Ven VG, Formisano E, Prvulovic D, Roeder CH, Linden DEJ. Functional connectivity as revealed by spatial independent component analysis of fMRI measurements during rest. Hum Brain Mapp 2004;22:165–78.
[40] Granger C. Investigating causal relations by econometric models and cross-spectral methods. Econometrica 1969;37:424–38.
[41] Friston KJ, Harrison L, Penny W. Dynamic causal modelling. Neuroimage 2003;19:1273–302.
[42] Barrat A, Barthélemy M, Vespignani A. Dynamical processes on complex networks. Cambridge University Press; 2008.
[43] Pastor-Satorras R, Vespignani A. Evolution and structure of the internet. A statistical physics approach. Cambridge University Press; 2007.
[44] Latora V, Marchiori M. Economic small-world behavior in weighted networks. Eur Phys J B-Condens Matter 2003;32:249–63.
[45] Watts DJ, Strogatz SH. Collective dynamics of 'small-world' networks. Nature 1998;393:440–2.
[46] Rubinov M, Sporns O. Complex network measures of brain connectivity: uses and interpretations. Neuroimage 2010;52:1059–69.
[47] Latora V, Marchiori M. Efficient behavior of small-world networks. Phys Rev Lett 2001:87.
[48] Sporns O. Networks of the brain. MIT Press; 2011.
[49] Newman M. Networks: an introduction: OUP Oxford; 2009.
[50] Strogatz S. Sync: the emerging science of spontaneous order. Penguin Books Limited; 2004.
[51] Humphries MD, Gurney K. Network 'small-world-ness': a quantitative method for determining canonical network equivalence. PLoS One 2008;3:e0002051.
[52] Bassett DS, Bullmore E. Small-world brain networks. Neuroscientist 2006;12:512–23.
[53] Huettel SA, Song AW, McCarthy G. Functional magnetic resonance imaging. 2nd ed. Sunderland, Mass: Sinauer Associates; 2008.
[54] Eguiluz VM, Chialvo DR, Cecchi GA, Baliki M, Apkarian AV. Scale-free brain functional networks. Phys Rev Lett 2005:94.
[55] Fox MD, Zhang D, Snyder AZ, Raichle ME. The global signal and observed anticorrelated resting state brain networks. J Neurophysiol 2009;101:3270–83.
[56] Weissenbacher A, Kasess C, Gerstl F, Lanzenberger R, Moser E, Windischberger C. Correlations and anticorrelations in resting-state functional connectivity MRI: a quantitative comparison of preprocessing strategies. Neuroimage 2009;47:1408–16.
[57] Bullmore E, Fadili J, Maxim V, Sendur L, Whitcher B, Suckling J, et al. Wavelets and functional magnetic resonance imaging of the human brain. Neuroimage 2004;23:S234–49.
[58] Shmueli K, van Gelderen P, de Zwart JA, Horovitz SG, Fukunaga M, Jansma JM, et al. Low frequency fluctuations in the cardiac rate as a source of variance in the resting-state fMRI BOLD signal. Neuroimage 2007;38:306.
[59] Bullmore ET, Bassett DS. Brain graphs: graphical models of the human brain connectome. Annu Rev Clin Psychol 2011;7:113–40.
[60] Achard S, Bullmore E. Efficiency and cost of economical brain functional networks. PLoS Comput Biol 2007;3:174–83.
[61] Schindler KA, Bialonski S, Horstmann M-T, Elger CE, Lehnertz K. Evolving functional network properties and synchronizability during human epileptic seizures. Chaos 2008:18.
[62] Ponten SC, Douw L, Bartolomei F, Reijneveld JC, Stam CJ. Indications for network regularization during absence seizures: weighted and unweighted graph theoretical analyses. Exp Neurol 2009;217:197–204.
[63] Barzegaran E, Joudaki A, Jalili M, Rossetti AO, Frackowiak RS, Knyazeva MG. Properties of functional brain networks correlate with frequency of psychogenic non-epileptic seizures. Front Hum Neurosci 2012;6:13.
[64] Ibrahim GM, Akiyama T, Ochi A, Otsubo H, Smith ML, Taylor MJ, et al. Disruption of Rolandic gamma-band functional connectivity by seizures is associated with motor impairments in children with epilepsy. Plos One 2012;7:8.
[65] Kuhnert MT, Elger CE, Lehnertz K. Long-term variability of global statistical properties of epileptic brain networks. Chaos 2010;20:9.
[66] Christodoulakis M, Anastasiadou M, Papacostas SS, Papathanasiou ES, Mitsis GD. Investigation of network brain dynamics from EEG measurements in patients with epilepsy using graph-theoretic approaches. IEEE 12th International Conference on Bioinformatics & Bioengineering; 2012. p. 303–8.
[67] Ponten SC, Bartolomei F, Stam CJ. Small-world networks and epilepsy: graph theoretical analysis of intracerebrally recorded mesial temporal lobe seizures. Clin Neurophysiol 2007;118:918–27.
[68] Kramer MA, Eden UT, Kolaczyk ED, Zepeda R, Eskandar EN, Cash SS. Coalescence and fragmentation of cortical networks during focal seizures. J Neurosci 2010;30:10076–85.

[69] Wu HH, Li XL, Guan XP. Networking property during epileptic seizure with multichannel EEG recordings. Advances in neural networks, 3973. Proceedings; 2006. p. 573–8 [Isnn 2006, Pt 3].
[70] Wilke C, Worrell G, He B. Graph analysis of epileptogenic networks in human partial epilepsy. Epilepsia 2011;52:84–93.
[71] Liao W, Zhang Z, Pan Z, Mantini D, Ding J, Duan X, et al. Altered functional connectivity and small-world in mesial temporal lobe epilepsy. Plos One 2010:5.
[72] Vlooswijk MCG, Vaessen MJ, Jansen JFA, de Krom M, Majoie HJM, Hofman PAM, et al. Loss of network efficiency associated with cognitive decline in chronic epilepsy. Neurology 2011;77:938–44.
[73] Zalesky A, Fornito A, Harding IH, Cocchi L, Yücel M, Pantelis C, et al. Whole-brain anatomical networks: does the choice of nodes matter? Neuroimage 2010;50:970.
[74] Salvador R, Suckling J, Coleman MR, Pickard JD, Menon D, Bullmore E. Neurophysiological architecture of functional magnetic resonance images of human brain. Cereb Cortex 2005;15:1332–42.
[75] Langer N, Pedroni A, Jaencke L. The problem of thresholding in small-world network analysis. Plos One 2013:8.
[76] Destrieux C, Fischl B, Dale A, Halgren E. A sulcal depth-based anatomical parcellation of the cerebral cortex. Neuroimage 2009;47:S151.